

# Elliptic instability in two-dimensional flattened Taylor–Green vortices

D. Sipp and L. Jacquin

ONERA, 29, Avenue de la Division Leclerc, BP 72, F-92322,  
Châtillon Cedex, France

(Received 13 August 1997; accepted 19 December 1997)

The aim of the present paper is to study three-dimensional elliptic instability in two-dimensional flattened Taylor–Green vortices, which constitutes a model problem for the topics of wake vortex dynamics. Shortwave asymptotics and classical linear stability theory are developed. Both approaches show that the flow is unstable. In particular, the structure of the most amplified growing mode is the same as that obtained in unbounded elliptical flows. The limits of the linear regime and the effects of the nonlinear interactions are characterized by means of a spectral Direct Numerical Simulation (DNS). © 1998 American Institute of Physics. [S1070-6631(98)02404-0]

## I. INTRODUCTION

The three-dimensional (3-D) elliptic instability in homogeneous elliptic flows is now well understood.<sup>1–3</sup> Extensions to nonhomogeneous cases, where the flow is only locally elliptical and where there may be boundary conditions, are not straightforward—we make a distinction between homogeneous basic flows which are unbounded with a uniform velocity gradient tensor and nonhomogeneous basic flows which can be bounded, like a flow in an elliptical cylinder, or unbounded.

However, linear stability results exist for such flows. Stability analyses of a Rankine or a Lamb vortex in an externally imposed plane strain field have already been achieved.<sup>4–6</sup> The mechanism of instability involved is a triadic resonance between two Kelvin waves of the same frequency and strain field. The same phenomenology occurs in a bounded elliptic cylinder.<sup>7</sup> The linear amplification rate is found to be nearly the same as in the homogeneous case. In fact, it has been shown<sup>2</sup> that the superposition of unstable unbounded Fourier modes leads to a growing inertial mode that satisfies the boundary conditions in an elliptic cylinder. So, in this particular case, a strict analogy exists between the homogeneous and the nonhomogeneous cases.

A recently developed theory by Lifschitz,<sup>8–10</sup> the so-called shortwave asymptotics, enables a generalization of the homogeneous flow theory to nonhomogeneous flows. It shows that elliptic stagnation points are always unstable with respect to short wavelength instabilities, no matter which type of flow surrounds them.

This paper is devoted to another example of nonhomogeneous flow subjected to an elliptic instability, the two-dimensional (2-D) Taylor–Green vortices, which is actually a solution of the viscous Navier–Stokes equations. It is defined by the following stream function:

$$\Psi = \frac{A(t) \sin b_x x \sin b_y y}{b_x^2 + b_y^2}$$

with  $A(t) = A_0 \exp(-\nu(b_x^2 + b_y^2)t)$ . The wave numbers  $b_x$  and  $b_y$  are related to the periodicities  $d_x$  and  $d_y$ :  $b_x = 2\pi/d_x$  and  $b_y = 2\pi/d_y$ . This flow, whose streamlines are represented in

Fig. 1, corresponds to an infinite array of counter-rotating vortices. There are elliptic and hyperbolic stagnation points. For example, at  $(x = d_x/4, y = d_y/4)$ , the flow is locally elliptical:  $U_x = -(\gamma + \epsilon)y$ ,  $U_y = +(\gamma - \epsilon)x$  with  $\gamma = A/2$  and  $\epsilon = A(b_y^2 - b_x^2)/2(b_y^2 + b_x^2)$ . The local ellipticity is  $E = \sqrt{(\gamma + \epsilon)/(\gamma - \epsilon)} = d_x/d_y$ , which is also the aspect ratio of the cells. The flow is locally hyperbolic at  $(x = 0, y = 0)$ :  $U_x = +\delta x$ ,  $U_y = -\delta y$  with  $\delta = Ab_x b_y / (b_x^2 + b_y^2)$ .

It is known, from shortwave asymptotics,<sup>8</sup> that both stagnation points are unstable. Therefore, we expect elliptic and hyperbolic instabilities. Thus care is needed since we are trying to study only elliptic instability.

Lundgren and Mansour<sup>11</sup> have performed a DNS of flattened 2-D Taylor–Green vortices and Bayly<sup>12,13</sup> gave some results on the linear stability with respect to short wavelength perturbations. In the present paper, the linear properties of this flow will be investigated with shortwave asymptotics (Sec. II A) and by applying the usual 3-D viscous linear stability analysis (Sec. II B). Then the nonlinear evolution of the growing mode will be studied by means of a Direct Numerical Simulation (DNS) (Sec. III).

## II. LINEAR STABILITY ANALYSIS

In this section, we neglect the slow viscous decay of the Taylor–Green flow by considering  $A(t)$  as constant and equal to 2.5. This assumes that the decay rate of the mean flow is slow compared to the growth rate of the instability.

The following cases have been considered:

- (1)  $E = 1$  with  $d_x = 1$ ,  $d_y = 1$ , where the elliptic points are now solid rotation points which are stable according to shortwave asymptotics;
- (2)  $E = 2$  with  $d_x = 2$ ,  $d_y = 1$ , where unstable elliptic and hyperbolic points coexist in the flow.

### A. Shortwave asymptotics

#### 1. General equations

Shortwave asymptotics were developed and applied by Lifschitz and Hameiri. In this section we review the basic theory. The reader is referred to Refs. 8–10 in which the

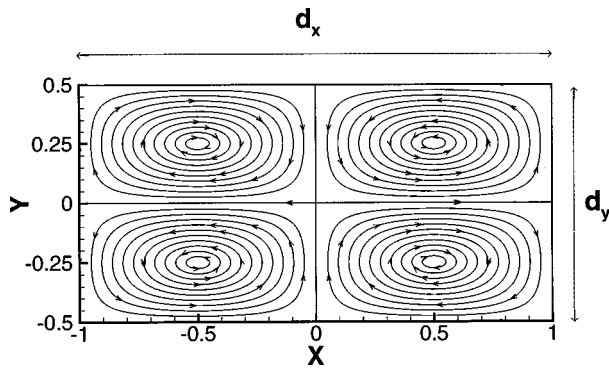


FIG. 1. Streamlines of 2-D Taylor–Green vortices. Case  $d_x=2, d_y=1, E=2$ .

whole theory is thoroughly explained and applied. This theory is now currently used in hydrodynamic stability studies of various flows.<sup>14–16</sup>

The steady basic flow  $\mathbf{U}(\mathbf{x})$  is perturbed by the following velocity field:

$$\mathbf{u}(\mathbf{x}, t) = \mathbf{a}(\mathbf{x}, t) \exp[i\eta^{-1}\phi(\mathbf{x}, t)],$$

where  $\eta$  is a small parameter. Introducing  $\mathbf{U}(\mathbf{x}) + \mathbf{u}(\mathbf{x}, t)$  in the inviscid incompressible Navier–Stokes equations and linearizing around the basic flow  $\mathbf{U}(\mathbf{x})$ , we get the following equation at lowest order in  $\eta$ :

$$(\partial_t + \mathbf{U} \cdot \nabla)\phi = 0,$$

which means that the phase field is passively advected.

The next-lowest-order terms yield the evolution equation for the velocity envelope function:

$$(\partial_t + \mathbf{U} \cdot \nabla)\mathbf{a} = \left( \frac{2\mathbf{k}\mathbf{k}^T}{|\mathbf{k}|^2} - \mathcal{I} \right) \mathcal{L}\mathbf{a},$$

where  $\mathbf{k} = \nabla\phi$ ,  $\mathcal{L}$  is the velocity gradient tensor,  $\mathcal{I}$  is the identity tensor, and the superscript  $T$  denotes the transpose. Lifschitz proved that the flow is unstable if this system of perturbation equations has any solutions whose amplitude increases unboundedly as  $t \rightarrow \infty$ .

This system evolves locally along particle trajectories, which means that it can be written in Lagrangian form. Thus, one considers a rapidly oscillating localized perturbation evolving along the trajectory  $\mathbf{X}(t)$  and characterized by a wave vector  $\mathbf{k}(t)$  and a velocity envelope  $\mathbf{a}(t)$ . For a steady flow, these quantities are governed by the following set of equations:

$$\frac{d\mathbf{X}}{dt} = \mathbf{U}(\mathbf{X}), \tag{1}$$

$$\frac{d\mathbf{k}}{dt} = -\mathcal{L}^T(\mathbf{X})\mathbf{k}, \tag{2}$$

$$\frac{d\mathbf{a}}{dt} = \left( \frac{2\mathbf{k}\mathbf{k}^T}{|\mathbf{k}|^2} - \mathcal{I} \right) \mathcal{L}(\mathbf{X})\mathbf{a}. \tag{3}$$

A sufficient criterion for instability is that this system has at least one solution for which the amplitude  $\mathbf{a}(t)$  unboundedly increases as  $t \rightarrow \infty$ .

These equations can be thought of as an extension of rapid distortion theory (RDT)<sup>17–19</sup> to nonhomogeneous flows. Although these equations seem similar, shortwave asymptotics is a different theory. In particular,  $\mathbf{k}$  and  $\mathbf{a}$  have different meanings in the two theories. It should be noted that the sufficient criterion of instability given above is not valid in RDT. Contrary to shortwave asymptotics, one has to integrate over  $\mathbf{k}$  to obtain the perturbation energy, which can decay, although some Fourier modes (typically a set of measure zero in  $\mathbf{k}$  space) have growing amplitudes.<sup>20</sup>

We restrict our analysis to the streamlines belonging to the cell  $(0 \leq x \leq d_x/2, 0 \leq y \leq d_y/2)$ . This cell contains one elliptic point at  $(x = d_x/4, y = d_y/4)$  and four hyperbolic points at  $(x = 0, y = 0)$ ,  $(x = 0, y = d_x/2)$ ,  $(x = d_x/2, y = 0)$ , and  $(x = d_x/2, y = d_y/2)$ . Note that all streamlines are closed except those bounding the cells. The origin of all these closed streamlines is taken as  $\mathbf{X}(t=0) = (x', d_y/4, 0)$  where  $d_x/4 \leq x' \leq d_x/2$ . The corresponding time period is denoted  $T(x')$ .

### 2. Floquet analysis for the differential equation governing $\mathbf{k}(t)$

For the case of closed streamlines, the matrix  $-\mathcal{L}^T[\mathbf{X}(t)]$  is periodic in time which means that the first-order linear-differential equation for the wave vector  $\mathbf{k}(t)$  (2) can be analyzed with Floquet theory. One looks for the eigenvalues/eigenvectors of the matrix  $\mathcal{H}[T(x')]$  where  $\mathcal{H}(t)$  is a matrix that satisfies

$$\frac{d\mathcal{H}}{dt} = -\mathcal{L}^T(\mathbf{X})\mathcal{H}$$

and

$$\mathcal{H}(0) = \mathcal{I}.$$

With the flow being 2-D, it is readily seen that  $\mathcal{H}_{31}[T(x')] = \mathcal{H}_{32}[T(x')] = 0$  and that  $[\lambda = 1, \mathbf{k}(0) = \mathbf{e}_z]$  is a trivial eigenvalue/eigenvector, which means that  $\mathcal{H}_{13}[T(x')] = \mathcal{H}_{23}[T(x')] = 0$  and  $\mathcal{H}_{33}[T(x')] = 1$ . Also, for a steady flow,  $d/dt[\mathbf{k} \cdot \mathbf{U}(\mathbf{X})] = 0$  along each streamline; hence  $\mathbf{k}(t) \cdot \mathbf{U}(\mathbf{X}(t)) = cte$ . Since  $\mathbf{U}(t=0)$  is parallel to  $\mathbf{e}_y$ , this implies that  $\mathcal{H}_{21}[T(x')] = 0$  and  $\mathcal{H}_{22}[T(x')] = 1$ . The trace of the matrix  $-\mathcal{L}^T$  being null, the determinant of  $\mathcal{H}[T(x')]$  is unity which implies that  $\mathcal{H}_{11}[T(x')] = 1$ . The matrix  $\mathcal{H}[T(x')]$  therefore reads

$$\mathcal{H}[T(x')] = \begin{pmatrix} 1 & \mathcal{H}_{12}(x') & 0 \\ 0 & 1 & 0 \\ 0 & 0 & 1 \end{pmatrix}.$$

The component  $\mathcal{H}_{12}(x')$  must be calculated numerically along each streamline. The results are shown in Fig. 2 for the case  $E=2$ . A similar result is obtained for the case  $E=1$ .

In the vortex center ( $x' \rightarrow d_x/4$ ), where the flow is locally homogeneous (in this case  $\mathcal{H}_{12} = 0$ ), the component  $\mathcal{H}_{12}(x')$  vanishes.

But, the more streamlines become distorted, the more  $\mathcal{H}_{12}(x')$  grows. This means that if  $\mathbf{k}(0) \cdot \mathbf{e}_y \neq 0$  the wave vector  $\mathbf{k}(t)$  will grow indefinitely. One may expect that the

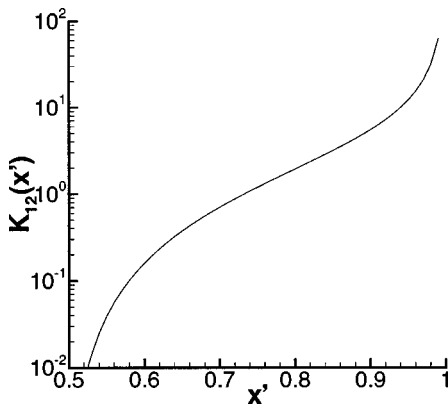


FIG. 2. Values of  $\mathcal{K}_{12}(x')$  for the case  $E=2, d_x=2, d_y=1$ .

wavy-perturbation dies out because of viscosity. Therefore, only the case  $\mathbf{k}(0) \cdot \mathbf{e}_y = 0$  is considered. Furthermore, the differential equation for  $\mathbf{a}(t)$  (3) is independent of the wave number  $|\mathbf{k}|$ . Consequently, the initial wave vector  $\mathbf{k}(0)$  only depends on the colatitude  $\theta$ :  $\mathbf{k}(0) = \sin(\theta)\mathbf{e}_x + \cos(\theta)\mathbf{e}_z$ . Besides, the first-order linear differential equation for  $\mathbf{a}(t)$  (3) can be analyzed with Floquet theory since  $\mathbf{k}(t)$  is periodic.

**3. Floquet analysis for the differential equation governing  $\mathbf{a}(t)$**

The same analysis is now applied for the differential equation governing  $\mathbf{a}(t)$  (3). We consider the matrix  $\mathcal{A}[T(x')]$ , where  $\mathcal{A}(t)$  satisfies

$$\frac{d\mathcal{A}}{dt} = \left( \frac{2\mathbf{k}\mathbf{k}^T}{|\mathbf{k}|^2} - \mathcal{I} \right) \mathcal{L}(\mathbf{X}) \mathcal{A}$$

and

$$\mathcal{A}(0) = \mathcal{I}.$$

A trivial eigenvalue/eigenvector of  $\mathcal{A}[T(x')]$  is  $[\mu=1, \mathbf{a}(0)=\mathbf{e}_z]$ . Because the determinant of  $\mathcal{A}[T(x')]$  is unity—it can be verified that the average over one period of the trace of  $(2\mathbf{k}\mathbf{k}^T/|\mathbf{k}|^2 - \mathcal{I})\mathcal{L}(\mathbf{X})$  is zero—the two remaining complex eigenvalues  $(\mu^1, \mu^2)$  where  $|\mu^1| \geq |\mu^2|$  must multiply to 1:  $\mu^1 \mu^2 = 1$ ; hence they are either complex conjugates of unit modulus or real and reciprocals. The system verifies  $d(k_i \mathcal{A}_{ij})/dt = 0$ , which proves that if  $[\mu, \mathbf{a}(0)]$  is an eigenvalue/eigenvector of  $\mathcal{A}[T(x')]$ , then  $[\mathbf{a}(0) \cdot \mathbf{k}(0)] \times (1 - \mu) = 0$ . This means that the two possible remaining eigenvectors are orthogonal to  $\mathbf{k}(0)$ . This result is consistent with shortwave asymptotics.

If the matrix  $\mathcal{A}[T(x')]$  is diagonalizable—a sufficient but not necessary condition for this is that  $(\mu^1, \mu^2, 1)$  are all distinct—the corresponding complex Floquet exponents  $(\sigma^1 = \sigma_r^1 + i\sigma_i^1, \sigma^2 = \sigma_r^2 + i\sigma_i^2)$ , defined as  $(\mu^1 = e^{\sigma^1 T(x')}, \mu^2 = e^{\sigma^2 T(x')})$  and therefore verifying  $\sigma_r^1 \geq \sigma_r^2$  and  $\sigma^1 + \sigma^2 = 0$ , enable us to conclude: if  $\sigma_r^1 > 0$  the streamline is unstable with respect to short wave asymptotics and if  $\sigma_r^1 \leq 0$ , it is stable.

When the matrix is not diagonalizable—a necessary but not sufficient condition for this is that equality arises among

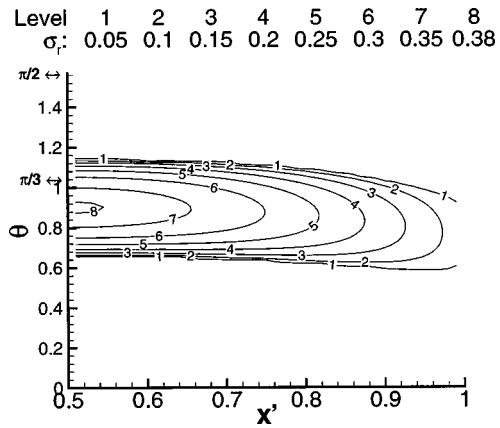


FIG. 3. Values of largest Floquet exponent  $\sigma_r^1$  in the  $(x', \theta)$  plane. Case  $E=2, d_x=2, d_y=1$ .

eigenvalues—the previous analysis fails. In a convenient normed basis, the matrix  $\mathcal{A}[T(x')]$  can be put in a Jordan form:

$$\begin{pmatrix} \mu & \lambda & 0 \\ 0 & \mu & 0 \\ 0 & 0 & 1 \end{pmatrix},$$

where  $\mu = \pm 1$ . The flow is always unstable but the growth rate is algebraic:  $|\lambda|/T(x')$  per period. Those cases will not be considered since we focus on exponentially growing instabilities; therefore we will only need to compute the two Floquet exponents  $(\sigma^1, \sigma^2)$ . Hence, the flow is exponentially unstable if  $\sigma_r^1 > 0$ . Finally, the colatitude angle  $\theta$  of the wave vector at  $t=0$  is taken in the interval  $[0, \pi/2]$  since the eigenvalues of  $\mathcal{A}[T(x')]$  are invariant with respect to the transformations  $\theta \rightarrow -\theta$  and  $\theta \rightarrow \pi - \theta$ .

The case  $E=1$  reveals that the closed streamlines are exponentially stable for all colatitude angles  $\theta$  of the initial wave vector  $\mathbf{k}(0)$  (we actually hope that we did not miss a narrow instability band since all cases are not studied but only a finite number of them) but the flow is actually algebraically unstable since for colatitudes  $\theta=0, \pi/2$  the matrix  $\mathcal{A}[T(x')]$  is not diagonalizable.

On the other hand, closed streamlines for the case  $E=2$  are unstable. The results are given in Fig. 3. In the center of the vortex, all the results, i.e., the amplification rate and the instability band of Bayly's homogeneous case when  $E=2$ , are recovered. As shown in Fig. 4, where the maximum values of  $\sigma_r$  are plotted versus  $x'$ , the amplification rate decreases as  $x'$  increases: The streamlines do not undergo exponential hyperbolic instability although the localized perturbation regularly goes through a hyperbolic region.

**4. Open cell-bounding streamlines**

Particles on streamlines that are not closed converge toward the hyperbolic stagnation points. Thus, one only needs to study these four particular points. Considering for instance the streamline  $\mathbf{X}(t) = \mathbf{X}(0) = (0,0,0)$ , one gets

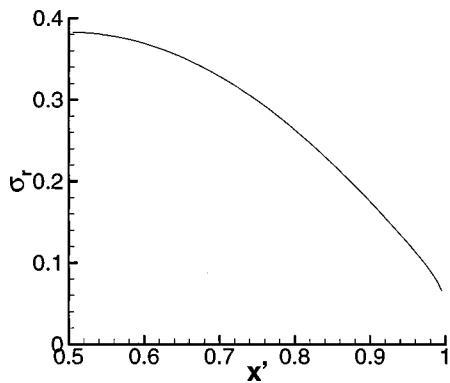


FIG. 4. Maximum values of  $\sigma_r^1$  vs the streamline parameter  $x'$ . Case  $E = 2$ ,  $d_x = 2$ ,  $d_y = 1$ .

$$-\mathcal{L}^T(\mathbf{X}) = \begin{pmatrix} -\frac{Ab_x b_y}{b_x^2 + b_y^2} & 0 & 0 \\ 0 & +\frac{Ab_x b_y}{b_x^2 + b_y^2} & 0 \\ 0 & 0 & 0 \end{pmatrix}.$$

$\mathbf{k}(0) = \mathbf{e}_y$  grows unboundedly which means that it will be damped by viscosity eventually and  $\mathbf{k}(0) = \mathbf{e}_x$  will tend to zero. Therefore, we will only determine the growth rate of  $\mathbf{a}(t)$  for the case  $\mathbf{k}(0) = \mathbf{k}(t) = \mathbf{e}_z$ . The matrix involved in (3) becomes

$$\left(\frac{2\mathbf{k}\mathbf{k}^T}{|\mathbf{k}|^2} - \mathcal{I}\right)\mathcal{L}(\mathbf{X}) = \begin{pmatrix} -\frac{Ab_x b_y}{b_x^2 + b_y^2} & 0 & 0 \\ 0 & +\frac{Ab_x b_y}{b_x^2 + b_y^2} & 0 \\ 0 & 0 & 0 \end{pmatrix}.$$

This shows that, whatever the value of  $E$ , the cell-bounding streamlines are unstable with amplification rate  $\sigma = Ab_x b_y / (b_x^2 + b_y^2) = \delta$ . For the case  $E = 1$ ,  $\sigma = \delta = 1.25$  and with  $E = 2$ ,  $\sigma = \delta = 1.00$ .

### B. Viscous linear stability theory

In this section we will perform a ‘‘classical’’ viscous linear stability analysis. The Reynolds number is defined on the circulation  $\Gamma$  over each cell:  $\Gamma = \oint u ds = Ad_x d_y / \pi^2$  which implies that  $\text{Re} = \Gamma / \nu = Ad_x d_y / (\pi^2 \nu)$ .

#### 1. Method

We consider a 3-D periodic flow, with periods  $(d_x, d_y, d_z)$ . The velocity field and pressure can therefore be expressed as follows:

$$\mathbf{u}(x, y, z, t) = \sum_{m, n, p} \hat{\mathbf{u}}(m, n, p, t) e^{I(mb_x x + nb_y y + pb_z z)},$$

$$p(x, y, z, t) = \sum_{m, n, p} \hat{p}(m, n, p, t) e^{I(mb_x x + nb_y y + pb_z z)}.$$

Let  $\mathbf{k}(m, n, p) = (k_x, k_y, k_z) = (mb_x, nb_y, pb_z)$ . The viscous incompressible Navier–Stokes equations read:

$$\frac{\partial \hat{\mathbf{u}}_\alpha}{\partial t} + \nu k^2 \hat{\mathbf{u}}_\alpha = -IP_{\alpha\beta} N_\beta, \tag{4}$$

where

$$P_{\alpha\beta} = \delta_{\alpha\beta} - \frac{k_\alpha k_\beta}{k^2},$$

$$N_\beta = \sum_{\mathbf{l}} \hat{u}_\beta(\mathbf{l}) k_\gamma \hat{u}_\gamma(\mathbf{k} - \mathbf{l}).$$

Introducing  $\hat{\mathbf{U}}(\mathbf{k}) + \hat{\mathbf{u}}(\mathbf{k})$  and linearizing around the basic flow, we get the following linear problem:

$$\frac{\partial \hat{\mathbf{u}}_\alpha}{\partial t} = -\nu k^2 \hat{\mathbf{u}}_\alpha + \sum_{\mathbf{l}} \left( -\hat{U}_\alpha(\mathbf{l}) I k_\gamma \hat{u}_\gamma(\mathbf{k} - \mathbf{l}) + \left( 2 \frac{k_\alpha k_\beta}{k^2} - \delta_{\alpha\beta} \right) I k_\gamma \hat{U}_\gamma(\mathbf{l}) \hat{u}_\beta(\mathbf{k} - \mathbf{l}) \right). \tag{5}$$

Because the basic flow is two dimensional, we can restrict our study to  $p = 1$  without loss of generality. Now, the Taylor–Green flow corresponds to a superposition of four elementary modes in spectral space:

$$\begin{aligned} \hat{U}_x(b_x, b_y, 0) &= \hat{U}_x(b_x, -b_y, 0) \\ &= -\hat{U}_x(-b_x, b_y, 0) \\ &= -\hat{U}_x(-b_x, -b_y, 0) = +\frac{A}{4I} \frac{b_y}{b_x^2 + b_y^2}, \\ \hat{U}_y(b_x, b_y, 0) &= -\hat{U}_y(b_x, -b_y, 0) \\ &= -\hat{U}_y(-b_x, b_y, 0) \\ &= \hat{U}_y(-b_x, -b_y, 0) = -\frac{A}{4I} \frac{b_x}{b_x^2 + b_y^2}. \end{aligned}$$

The sum over  $\mathbf{l}$  in the linear operator involved on the right-hand side of Eq. (5) reduces therefore to four terms. Besides, as pointed out by Bayly,<sup>13</sup> the eigenmodes can be decomposed into two independent subsets: the even modes where  $m + n$  is even and the odd modes where  $m + n$  is odd. This comes from the fact that each mode  $(m, n)$  is only coupled with the four neighboring modes  $(m - 1, n - 1)$ ,  $(m - 1, n + 1)$ ,  $(m + 1, n - 1)$ ,  $(m + 1, n + 1)$ .

We represent this linear operator with a matrix, in which each component corresponds to a mode interaction. Thanks to viscosity, we truncate that matrix and solve the eigenvalue/eigenvector problem numerically. When looking for the odd modes eigenvalues on a DEC alpha server 8400 5/300 with 8 processors, it takes 19 h of computation when the matrix size is  $6560 \times 6560$ , which corresponds to  $-40 \leq m \leq 40$  and  $-40 \leq n \leq 40$ .

The eigenvalues and eigenvectors  $[\sigma, \tilde{\mathbf{u}}(\mathbf{k})]$  found are such that  $\mathbf{u}(t) = e^{\sigma t} \tilde{\mathbf{u}}(\mathbf{k})$  is a solution of the linearized Navier–Stokes equations (5).

The basic flow is linear with respect to  $A$ . This means that the eigenvalues are proportional to  $A$  and that the structure of the eigenmodes do not depend on  $A$ . Thus, an eigenmode developing on a viscous decaying Taylor–Green flow

remains an eigenmode for all time, the amplification rate decreasing as  $A(t)$ . This property will be used in Sec. III.

**2. Problems connected with truncation of the Fourier modes**

As we solve the linear problem with a finite number of Fourier modes, we have to be careful with the interpretation of the eigenvalues/eigenvectors given by this numerical method. An eigenvalue/eigenvector couple is valid only if the eigenvector concentrates all of its energy in the modes with small wave number  $(m,n)$ . For example, suppose that we represent the modes verifying  $-40 \leq m, n \leq 40$ . With our numerical method we will obtain 6560 couples of eigenvalues/eigenvectors. Now, we have to look at the spectrum of each eigenvector. A rough criteria of validity in this case could be: 99% of the energy should be contained in the modes verifying  $-20 \leq m, n \leq 20$ , i.e., in the lowest part of the handled spectrum. If not, part of the energy lies in the upper part of the spectrum and therefore truncation invalidates the corresponding eigenvector. Hence, for each calculation, we have to check the validity of each couple carefully.

Finally, this truncation method only gives a few of the valid eigenvalues/eigenvectors. In the following, we suppose that this set contains the most amplified modes (so that we can conclude whether the flow is stable or not). This is true when viscosity is large, since viscosity stabilizes the short-wave perturbations. In Secs. II B 3 and II B 5, this argument holds. But, in Sec. II B 6, we perform an inviscid stability analysis. In this case, viscosity cannot be put forward and nothing enables us to state that the calculated set of valid modes includes the most unstable ones.

**3. The case  $E=1$**

The numerical problem was solved for the following set of parameters:  $E=1, d_x=1, d_y=1, d_z=0.5625, Re=2500$ . The vertical wavelength  $d_z=0.5625$  corresponds to the most unstable configuration. The eigenvalues are plotted in Fig. 5 for both odd and even modes (symbols labeled “general case”). Each symbol represents one eigenvalue in the  $(\sigma_r, \sigma_i)$  plane. The striking fact here is that the flow is unstable: There are four unstable odd modes and three unstable even modes. The structure of a typical unstable eigenmode is given in Fig. 6 where we have shown the norm of the horizontal vorticity in the plane  $(x,y)$ . All these eigenmodes are localized on the planes separating the cells, where as shown before with short wave asymptotics, streamlines are unstable. Therefore, the instability is due to the hyperbolic stagnation points.

However, this is a spurious phenomenon when studying instabilities occurring in the center of the vortices. Hence, we will now try to eliminate this “hyperbolic” instability.

**4. Slip conditions**

In a recent paper,<sup>11</sup> Lundgren suggests imposing the following consistent set of symmetry conditions in spectral space for all  $(m,n,p)$ :

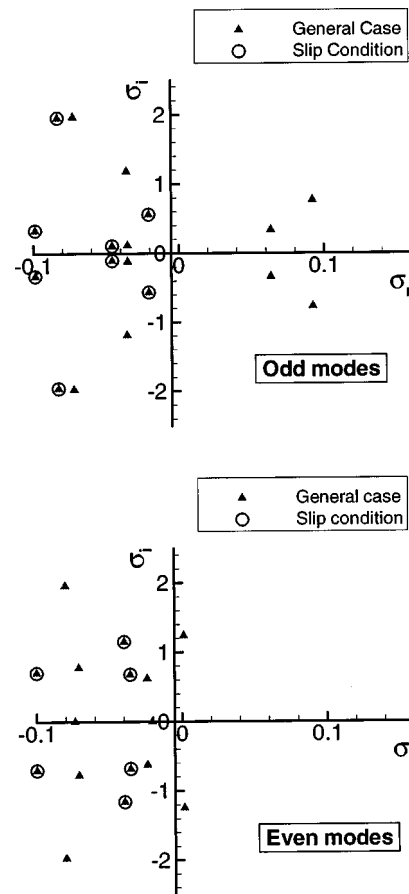


FIG. 5. Odd and even mode eigenvalues in the  $(\sigma_r, \sigma_i)$  plane. Case  $E=1, d_x=1, d_y=1, d_z=0.5625, Re=2500$ .

$$\begin{aligned}
 \hat{u}_x(-m,n,p) &= -\hat{u}_x(m,n,p), \\
 \hat{u}_y(-m,n,p) &= +\hat{u}_y(m,n,p), \\
 \hat{u}_z(-m,n,p) &= +\hat{u}_z(m,n,p), \\
 \hat{u}_x(m,-n,p) &= +\hat{u}_x(m,n,p), \\
 \hat{u}_y(m,-n,p) &= -\hat{u}_y(m,n,p), \\
 \hat{u}_z(m,-n,p) &= +\hat{u}_z(m,n,p).
 \end{aligned}
 \tag{6}$$

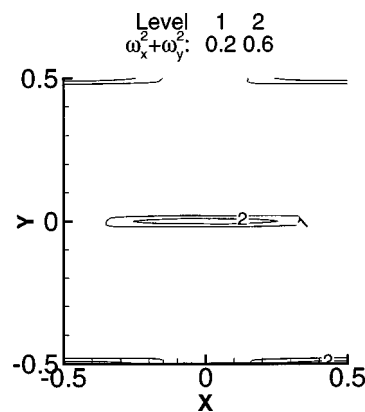


FIG. 6. Iso- $\omega_x^2 + \omega_y^2$  in a cut  $z = cte$  of a typical unstable eigenfunction. Case  $E=1, d_x=1, d_y=1, d_z=0.5625, Re=2500$ .

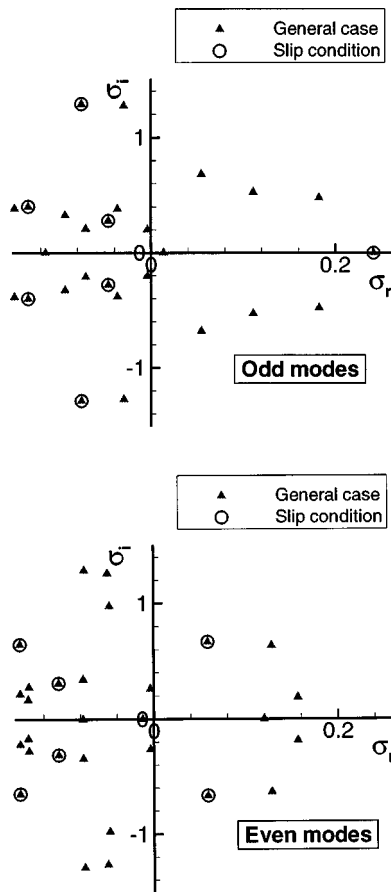


FIG. 7. Odd and even mode eigenvalues in the  $(\sigma_r, \sigma_i)$  plane. Case  $E=2$ ,  $d_x=2$ ,  $d_y=1$ ,  $d_z=1.84375$ ,  $Re=2500$ .

We are going to show that these symmetry conditions stabilize the flow  $E=1$ , therefore removing the spurious unstable hyperbolic modes.

It can be shown that the viscous Navier–Stokes equations conserve these symmetries and that the corresponding eigenvalues just form a subset of the general case eigenvalues.

These conditions imply that the flow slips along the planes separating the vortices:  $u_x=0$  on the planes  $x = n_x d_x/2 \forall n_x$  and  $u_y=0$  on the planes  $y = n_y d_y/2 \forall n_y$ .

When applying these slip conditions, the flow with  $E=1$  is stabilized as it is shown in Fig. 5 where the circles represent the eigenvalues that verify these slip conditions.

**5. The case  $E=2$**

We now look at the elliptic instability that should develop for the case  $E=2$ . Calculations are performed for the case  $d_x=2$ ,  $d_y=1$ ,  $d_z=1.84375$ ,  $Re=2500$ . Again, the vertical size of the box corresponds to the most unstable configuration. The eigenvalues are given in Fig. 7. It can be seen that the flow is unstable. Yet the slip condition removes seven out of eight unstable odd modes and five out of seven unstable even modes. The typical structure of the remaining unstable modes is given in the upper plot of Fig. 8: The horizontal vorticity is concentrated on the vortex centers and there is very little vorticity on the planes separating the vor-

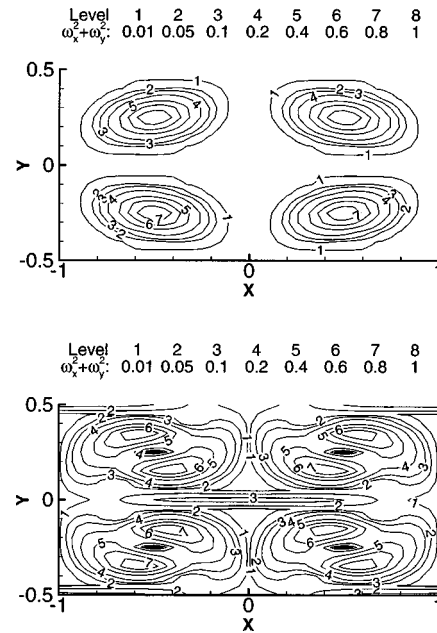


FIG. 8. Upper plot: iso- $(\omega_x^2 + \omega_y^2)$  in a  $z=cte$  cut of a typical eigenfunction of the slip-condition subset (“elliptic” mode). Lower plot: the same for a typical function not belonging to that subset (“hyperbolic” mode). Case  $E=2$ ,  $d_x=2$ ,  $d_y=1$ ,  $d_z=1.84375$ ,  $Re=2500$ .

tices. On the other hand, in the lower plot of Fig. 8, we can see that the vorticity on the removed eigenmodes is also very strong on these planes. In conclusion, the slip conditions are an efficient means to eliminating hyperbolic instability modes in Taylor–Green flows.

The spectral structure of the remaining unstable odd mode is given in Table I. For each Fourier mode  $\hat{\mathbf{u}}(m,n)e^{I(mb_x x + nb_y y + b_z z)}$ , the first and second columns give wave numbers  $m$  and  $n$ , the third to fifth columns give  $\hat{\mathbf{u}}$  normalized so that  $\sum_{m,n} |\hat{\mathbf{u}}(m,n)|^2 = 1$ , the sixth column gives the percentage of energy  $|\hat{\mathbf{u}}(m,n)|^2$ , and the last column the cumulative sum of these percentages. It is seen that

TABLE I. Spectral structure of the most amplified odd mode. For each Fourier mode, the first and second columns give the wave numbers  $m$  and  $n$ , the third to fifth columns give  $\hat{u}_x, \hat{u}_y, \hat{u}_z$ , the sixth column gives the percentage of energy in the corresponding  $(m,n)$  mode, and the last column gives the cumulative sum. Case  $E=2$ ,  $d_x=2$ ,  $d_y=1$ ,  $d_z=1.84375$ ,  $Re=2500$ .

$m$	$n$	$\hat{u}_x$	$\hat{u}_y$	$\hat{u}_z$	Energy fraction (%)	Energy sum (%)
-1	0	0.312	0	0.287	17.98	17.98
1	0	-0.312	0	0.287	17.98	35.96
0	1	0	-0.139	0.256	8.45	44.41
0	-1	0	0.139	0.256	8.45	52.86
1	-2	0.246	0.053	-0.031	6.45	59.31
-1	-2	-0.246	0.053	-0.031	6.45	65.77
-1	2	-0.246	-0.053	-0.031	6.45	72.22
1	2	0.246	-0.053	-0.031	6.45	78.67
-2	1	0.113	0.164	-0.093	4.83	83.5
2	1	-0.113	0.164	-0.093	4.83	88.34
2	-1	-0.113	-0.164	-0.093	4.83	93.17
-2	-1	0.113	-0.164	-0.093	4.83	98.0
...	...	...	...	...	...	...

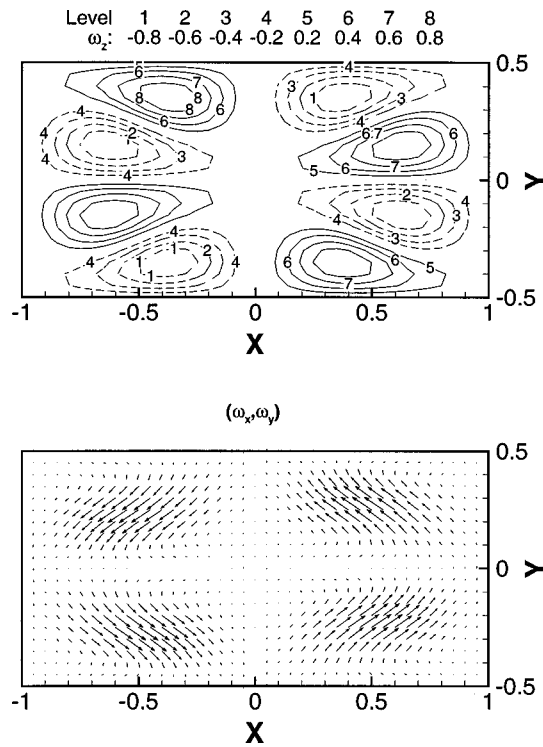


FIG. 9. Vertical vorticity  $\omega_z$  (upper plot) and horizontal vorticity  $(\omega_x, \omega_y)$  (lower plot) of the most amplified eigenfunction. To be compared with Figs. 2 and 3 of Waleffe's unbounded elliptic instability. Case  $E=2$ ,  $d_x=2$ ,  $d_y=1$ ,  $d_z=1.84375$ ,  $Re=2500$ .

12 Fourier modes contain 98% of the energy of the eigenmode. The involved Fourier modes are all long wavelength ( $|m| \leq 2$  and  $|n| \leq 2$ ). An important consequence of this result is that very little resolution is needed in spectral space to represent the growing mode when performing the DNS in Sec. III.

The corresponding horizontal and vertical vorticity in physical space are given in Fig. 9. These two pictures can be compared with Figs. 2 and 3 of Waleffe's paper.<sup>2</sup> The structure of the mode in each cell is roughly the same as that obtained in homogeneous elliptic flows: The vertical vorticity forms a dipole whose axis is aligned with the stretching direction and the horizontal vorticity is oriented in the same direction. Furthermore, for both cases the mode is stationary. The amplification rate  $\sigma = 0.2414$  has to be compared with 0.3825, obtained both with the corresponding  $E=2$  inviscid homogeneous case and with inviscid shortwave asymptotics applied in the center of the vortex (see Figs. 3 and 4). This discrepancy is mainly due to the fact that the vertical wave number  $k_z = 2\pi/d_z = 3.41$  is not asymptotically large (see Sec. II B 6). Also, one could invoke viscosity but viscosity remains weak for our case where  $Re=2500$ .

In Fig. 10 we give a plot of the ten most amplified eigenvalues  $\sigma_r$ —of the slip-condition subset—for both odd and even modes versus vertical wave number  $k_z$ . The arrow locates the vertical wave number corresponding to  $d_z = 1.84375$ , used until now for the  $E=2$  case. These intricate plots represent the linear mode interactions in this flow. Figure 11 gives a zoom on the area shown by a circle in Fig. 10:

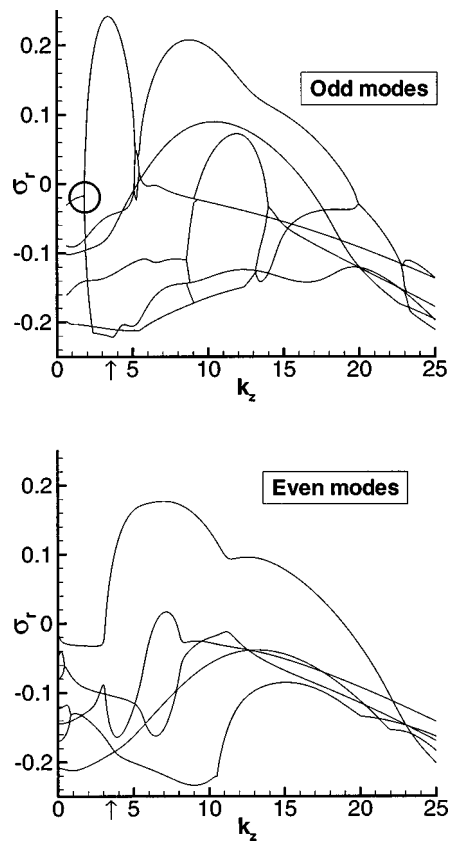


FIG. 10. Odd and even mode eigenvalues in the  $(k_z, \sigma_r)$  plane. An arrow shows the case  $d_z = 1.84375$ . Case  $E=2$ ,  $d_x=2$ ,  $d_y=1$ ,  $Re=2500$ .

We can see in the  $(\sigma_r, \sigma_i)$  plane two eigenvalues collapsing and giving rise to the most amplified odd mode.

**6. Link between shortwave asymptotics and classical linear stability theory**

The shortwave asymptotics describe inviscid shortwave instabilities. The results were given in Sec. II A. In order to compare the theory with the classical linear theory used in this section, we solve the eigenvalue/eigenvector problem with the following set of parameters:  $d_x=2$ ,  $d_y=1$ ,  $d_z=0.25$ ,  $\nu=0$ , which means that  $Re=\infty$ . The periods  $d_x$  and  $d_y$  correspond to the usual basic flow  $E=2$ . The period  $d_z$  is smaller compared to the preceding cases in order to describe

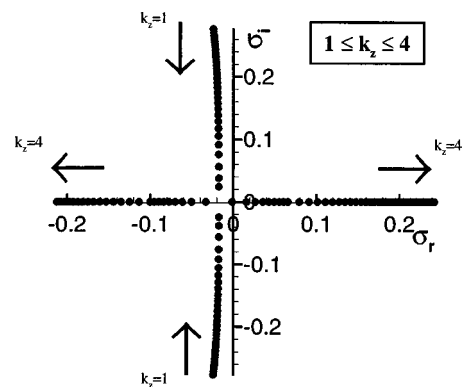


FIG. 11. Magnification of the  $(\sigma_r, \sigma_i)$  plane in the area shown by the circle in Fig. 10. Case  $E=2$ ,  $d_x=2$ ,  $d_y=1$ ,  $Re=2500$ .

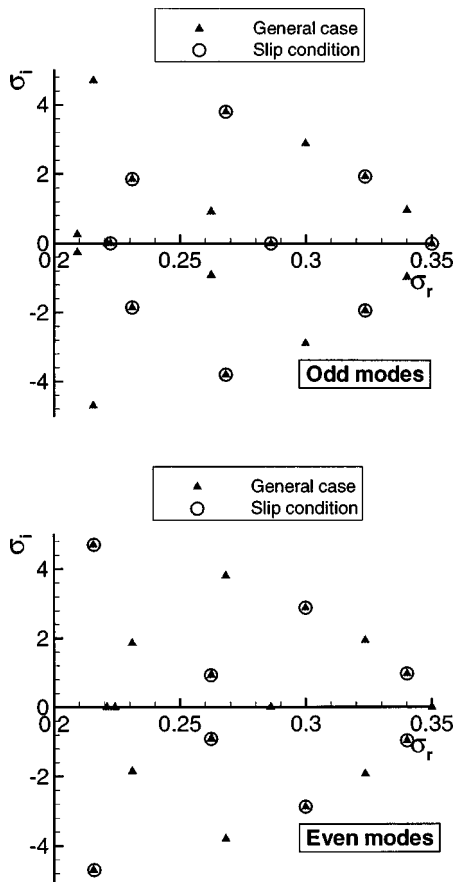


FIG. 12. Odd and even mode Eigenvalues in the  $(\sigma_r, \sigma_i)$  plane. Case  $E=2, d_x=2, d_y=1, d_z=0.25, \nu=0$ .

perturbations with shorter wavelengths. The general case eigenvalues have been computed with a spectral resolution of  $-40 \leq m, n \leq 40$ . The slip-condition eigenvalues have been computed with an even higher resolution to check the quality of the results of the general case eigenvalues. The calculation has been performed to account for the following modes:  $-80 \leq m, n \leq 80$ . This was possible because of the new symmetries involved in the problem. The size of the matrix is approximately the same as in the previous calculation.

Results are given in Fig. 12. The amplification rate of the most unstable mode is 0.3500, obtained with both calculations. This is close to the 0.3825 amplification rate predicted with shortwave asymptotics.

The spectral structure of the most unstable odd mode, part of which is given in Table II, shows that 99% of the energy is concentrated in the  $(m, n)$  modes verifying  $-14 \leq m, n \leq 14$ . The corresponding horizontal and vertical vorticity in physical space are given in Fig. 13. We can see that it is an elliptic mode. The picture given here is very close to the unbounded homogeneous case.<sup>2</sup>

As mentioned in Sec. II B 2, we have to be cautious with the interpretation of the results. Since viscosity has been set to zero, shortwave perturbations are not stabilized. Therefore, the pictures in Fig. 12 may not be exhaustive: There may be an eigenvalue/eigenvector couple (which we cannot describe with the spectral resolution employed), which is even more unstable than those exhibited. This is a little dis-

TABLE II. Spectral structure of the most amplified odd mode. The first and second columns give the wave numbers  $|m|$  and  $|n|$ , the third column gives the percentage of energy in the corresponding  $(|m|, |n|)$  modes, and the last column gives the cumulative sum. Case  $E=2, d_x=2, d_y=1, d_z=0.25, Re=\infty$ .

$ m $	$ n $	Energy fraction (%)	Energy sum (%)
9	2	5.6	5.6
9	4	4.7	10.3
7	6	4.2	14.5
5	8	3.5	18.0
7	4	3.4	21.4
10	1	3.2	24.6
1	10	3.0	27.6
10	3	3.0	30.6
...	...	...	...
14	1	0.3	96.5
...	...	...	...
14	3	0.2	98.6
...	...	...	...
7	12	0.1	99.0
...	...	...	...

turbing, but the following conclusion still holds: We have discovered an inviscid elliptic mode, whose amplification rate is close to the value predicted by shortwave asymptotics. The matching will be more exact if we use an even shorter

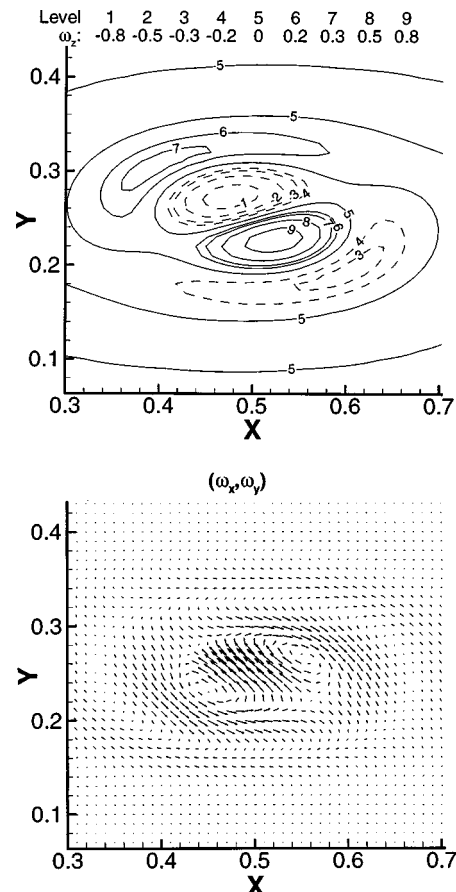


FIG. 13. Vertical vorticity  $\omega_z$  (upper plot) and horizontal vorticity  $(\omega_x, \omega_y)$  (lower plot) of the most amplified odd mode (in upper right cell). To be compared with Figs. 2 and 3 of Waleffe's unbounded elliptic instability. Case  $E=2, d_x=2, d_y=1, d_z=0.25, \nu=0$ .

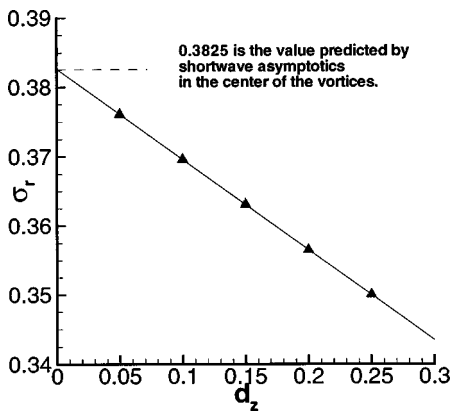


FIG. 14. Amplification rate of the most unstable odd mode of the slip condition subset vs vertical wavelength  $d_z$ . Case  $E=2, d_x=2, d_y=1, \nu=0$ .

wavelength  $d_z$ . To prove this statement, we have done a series of calculations with the vertical wavelength  $d_z$  set to  $d_z=0.05, 0.1, 0.15, 0.2, 0.25$ . Only the slip condition modes have been calculated because of memory constraints. We focus on the most amplified odd mode. The smaller the value of  $d_z$ , the more spectral resolution we need: For example, in the case  $d_z=0.1$ , we need the wave numbers verifying  $-29 \leq m, n \leq 29$  to store 99% of the energy of the mode. We checked that for each value of  $d_z$ , the mode is elliptic, i.e., the mode is localized on the center of the vortices and the structure of the horizontal and vertical vorticity is the same as in Waleffe.<sup>2</sup> The corresponding amplification rate versus the vertical wavelength  $d_z$  is given in Fig. 14. A straight line was fitted to the observations and the extrapolation of this line to  $d_z=0$  gives  $\sigma_r=0.3825$ , which is the same as the value predicted by shortwave asymptotics in the center of the vortices (this extrapolation method has already been used by Bayly<sup>13</sup>). This proves that shortwave asymptotics are totally consistent with classical linear theory.

### III. THE NONLINEAR REGIME

#### A. The code

We use a Fourier spectral code that solves the incompressible Navier–Stokes equations (4). The nonlinear term is directly computed in spectral space by evaluation of convolution sums. Time advancement is achieved with a compact third-order Runge–Kutta scheme. Time-discretization and truncation (a finite number of Fourier modes are used) are the only approximations achieved. Viscosity is used through the damping term  $e^{-\nu k^2 t}$  to filter the shortwave contribution lying outside the calculation domain.

#### B. Results for the case $E=2$

A calculation was performed with  $E=2, d_x=2, d_y=1$ , and  $d_z=1.84375$ . The Reynolds number is 2500. The viscous cutoff is given by  $k_c=1/\sqrt{\nu}=70$ . The size of the calculation box is  $25 \times 25 \times 17$  which, thanks to the high symmetries achieved in spectral space, enables us to represent the following modes:  $-24 \leq m \leq 24, -24 \leq n \leq 24$  and  $-16 \leq p \leq 16$  or, in terms of wavelengths,  $-75 \leq k_x \leq 75, -150 \leq k_y$

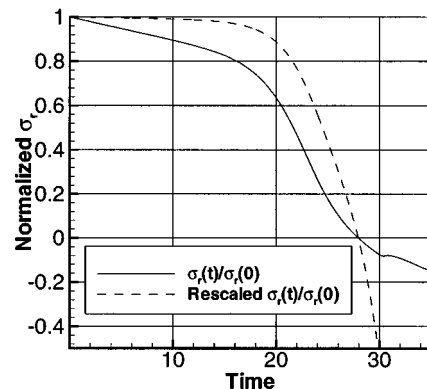
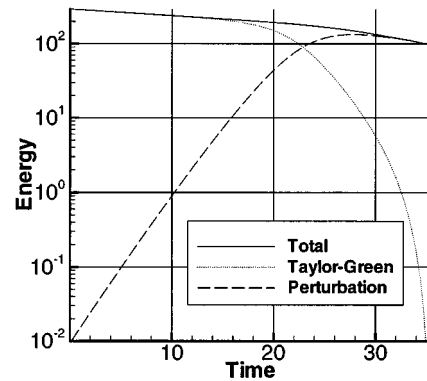
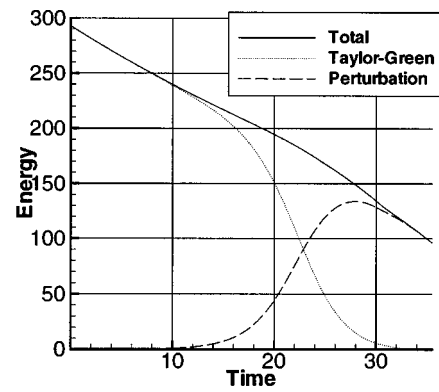


FIG. 15. Upper plot: total energy (solid line), Taylor Green energy (dotted line), and perturbation energy (dashed line) vs time. Middle plot: the same in log scale. Lower plot: normalized amplification rate  $\sigma_r(t)/\sigma_r(0)$  (solid line). The dashed line is the same but rescaled to take account for viscous decay of the basic flow. Case  $E=2, d_x=2, d_y=1, d_z=1.84375, Re=2500$ .

$\leq 150, -55 \leq k_z \leq 55$ . This is certainly not sufficient when a strong cascade develops, but this is not the case and the calculation is valid for a long time.

We initialize the calculation with the four Taylor–Green modes with  $A_0=2.5$  plus the most amplified odd mode. The structure of this mode and its theoretical amplification rate is given by the linear stability analysis. For the present case:  $\sigma_r=0.2414$ .

The results of the calculations are given in Figs. 15 and 16.

The two upper plots in Fig. 15 give the time evolution of the total energy in the box (solid line), the energy of the four modes that form the Taylor–Green flow (dotted line), and

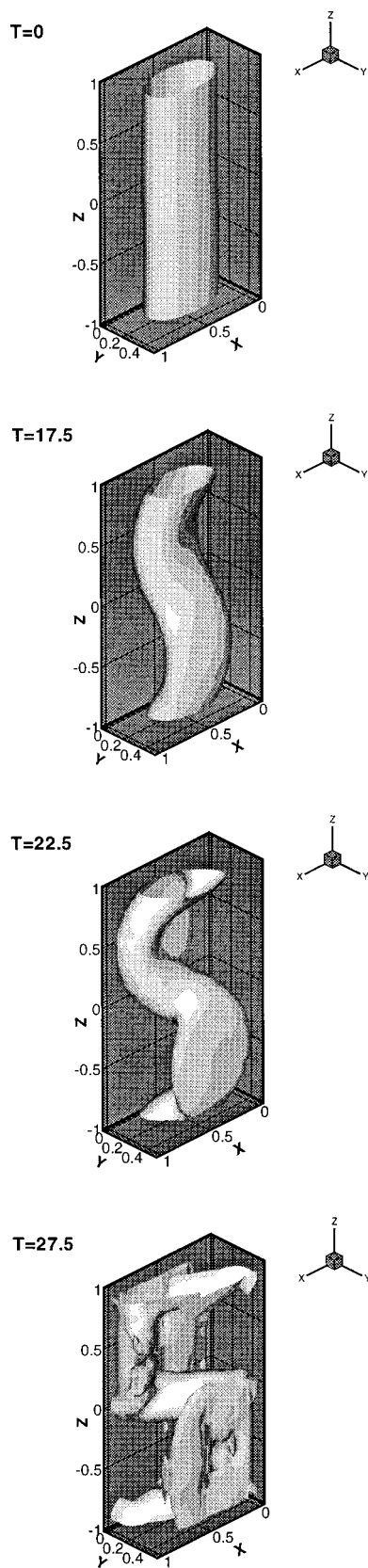


FIG. 16. Time evolution of iso-vorticity surfaces.

the remaining energy called the perturbation energy (dashed line). These two plots represent the same data, the first in linear scale, the second in log scale. The total energy is decreasing because of viscosity. The perturbation energy,

which was initially three orders of magnitude smaller than the basic flow energy, undergoes a dramatic increase at the expense of the basic flow. For example, at time  $T=23$ , there is as much energy in the perturbation as in the Taylor–Green vortices. At time  $T=30$ , there is nearly no energy any more in the Taylor–Green vortices. The plot in log scales shows that the instability is exponential: The initial slope of the perturbation energy curve (divided by two to transform energy growth rates into amplitude growth rates) is exactly that predicted by linear theory (which proves that our code works well). The lower plot in Fig. 15 represents, in solid line, the energy amplification rate (again divided by two) normalized by the initial theoretical linear stability amplification rate. This value is decreasing because viscosity is eroding the basic flow [remember that eigenvalues are proportional to  $A(t)$ ] and because of nonlinearities. In the lower plot, we have also represented in a dashed line, a rescaled version of the amplification rate:  $\sigma_r^{rs}(t) = \sigma_r(t)A(0)/\sigma_r(0)A(t)$ , where  $A(t)$  is the value computed at time  $t$ . If there were no nonlinearities, this quantity should be equal to  $\sigma_r^{rs}(t) = 1$  for all time. As we can see,  $\sigma_r^{rs}(t)$  is close to 1 for  $T \leq 20$ , which corresponds to  $E^P(t)/E^{TG}(t) \leq 1/3$ , where  $E^P(t)$  is the perturbation energy and  $E^{TG}(t)$  is the Taylor–Green energy. This quantity then decreases drastically because of nonlinear effects: The energy of the perturbation is of the same order of magnitude as the energy of the Taylor–Green vortices.

The four plots of Fig. 16 represent time evolution of iso-values of total vorticity in one cell. The initial elliptic vortex ( $T=0$ ) undergoes a sinusoidal instability ( $T=17.5$ ) until the vortex encounters the cell-separating boundaries ( $T=22.5$  and  $T=27.5$ ). The picture of the early stages of that DNS ( $T=0$  and  $T=17.5$ ) is consistent with Leweke’s shortwave instabilities observations in a vortex pair.<sup>21</sup>

#### IV. CONCLUSION

We have achieved the linear stability analysis for the two cases  $E=1$  and  $E=2$ . A comparison between shortwave asymptotics and classical linear stability theory has been achieved. Although the domain of validity of the two theories is completely different (short wavelength for shortwave asymptotics and long wavelength for viscous classical linear theory), this study reveals that they are consistent. Shortwave asymptotics have proved that all closed streamlines of  $E=1$  flow are exponentially stable whereas the planes separating each vortex are strongly unstable ( $\sigma_r = \delta = 1.25$ ). These results are consistent with the application of classical linear theory. Imposing slip conditions enables us to eliminate these unstable modes. For the case  $E=2$ , shortwave asymptotics show that streamlines in the center of the vortex are the most unstable with  $\sigma_r = 0.3825$  (these results are totally consistent with Bayly’s homogeneous  $E=2$  case) and that this amplification rate decreases when going outward. The planes separating the vortices are also highly unstable ( $\sigma_r = \delta = 1.00$ ). Again, we remove the “hyperbolic” unstable modes in the classical linear theory by imposing slip conditions on these planes. The remaining most amplified

mode is stationary and its structure is the same as that found in Waleffe's homogeneous elliptic instability. The nonlinear regime has then been studied by means of a spectral DNS. It has been shown that the elliptic instability develops into a sinusoidal perturbation that grows until it encounters the slip-condition boundaries. The amplification rate is exactly predicted by linear theory for moderate perturbation energy.

In brief, we have clearly identified elliptic instability in this nonhomogeneous Taylor–Green flow. We expect similar results with more realistic flows, e.g., a vortex pair that was created by the roll-up of a vortex sheet. As mentioned earlier, inviscid stability analyses already exist for a strained Lamb vortex, i.e., a model problem for the counter-rotating vortex pair, but quantitative results concerning viscosity effects are still lacking. This will be our next concern.

### ACKNOWLEDGMENTS

We would like to thank C. Cambon and S. Leblanc for fruitful discussions on this problem.

- <sup>1</sup>B. J. Bayly, "Three-dimensional instability of elliptical flow," *Phys. Rev. Lett.* **57**, 2160–2163 (1986).
- <sup>2</sup>F. Waleffe, "On the three-dimensional instability of strained vortices," *Phys. Fluids A* **2**, 76–80 (1990).
- <sup>3</sup>M. J. Landman and P. G. Saffman, "The three-dimensional instability of strained vortices in a viscous fluid," *Phys. Fluids* **30**, 2339–2342 (1987).
- <sup>4</sup>D. W. Moore and P. G. Saffman, "The instability of a straight vortex filament in a strain field," *Proc. R. Soc. London, Ser. A* **346**, 413–425 (1975).
- <sup>5</sup>C. Y. Tsai and S. E. Widnall, "The stability of short waves on a straight vortex filament in a weak externally imposed strain field," *J. Fluid Mech.* **73**, 721–733 (1976).
- <sup>6</sup>A. C. Robinson and P. G. Saffman, "Three-dimensional stability of an elliptical vortex in a straining field," *J. Fluid Mech.* **142**, 451–466 (1984).

- <sup>7</sup>F. Waleffe, "The 3D instability of a strained vortex and its relation to turbulence," Ph.D. thesis, MIT, July 10, 1989.
- <sup>8</sup>A. Lifschitz and E. Hameiri, "Local stability conditions in fluid dynamics," *Phys. Fluids A* **3**, 2644–2651 (1991).
- <sup>9</sup>A. Lifschitz and E. Hameiri, "Localized instabilities of vortex rings with swirl," *Commun. Pure Appl. Math.* **46**, 1379–1408 (1993).
- <sup>10</sup>A. Lifschitz, "On the instability of certain motions of an ideal incompressible fluid," *Adv. Appl. Math.* **15**, 404–436 (1994).
- <sup>11</sup>T. S. Lundgren and N. M. Mansour, "Transition to turbulence in an elliptic vortex," *J. Fluid. Mech.* **307**, 43–62 (1996).
- <sup>12</sup>B. J. Bayly, "Three-dimensional centrifugal-type instabilities in inviscid two-dimensional flows," *Phys. Fluids* **31**, 56–64 (1988).
- <sup>13</sup>B. J. Bayly, "Computations of broad-band instabilities in a class of closed-streamline flows," in *Mathematical Aspects of Vortex Dynamics*, edited by R. E. Caflisch (SIAM, Philadelphia, 1989), pp. 50–58.
- <sup>14</sup>B. J. Bayly, D. D. Holm, and A. Lifschitz, "Three-dimensional stability of elliptical vortex columns in external strain flows," *Philos. Trans. R. Soc. London, Ser. A* **354**, 895–926 (1996).
- <sup>15</sup>N. R. Lebovitz and A. Lifschitz, "Short-wavelength instabilities of Riemann ellipsoids," *Philos. Trans. R. Soc. London, Ser. A* **354**, 927–950 (1996).
- <sup>16</sup>S. Leblanc and C. Cambon, "On the three-dimensional instabilities of plane flows subjected to Coriolis force," *Phys. Fluids* **9**, 1307–1316 (1997).
- <sup>17</sup>C. Cambon, "Etude spectrale d'un champ turbulent incompressible soumis à des effets couplés de déformation et de rotation imposés extérieurement," Ph.D. thesis, Univ. Lyon I, France, 1982.
- <sup>18</sup>C. Cambon, C. Teissèdre, and D. Jeandel, "Etude d'effets couplés de déformation et de rotation sur une turbulence homogène," *J. Méc. Théo. Appl.* **4**, 629–657 (1985).
- <sup>19</sup>C. Cambon, J.-P. Benoit, L. Shao, and L. Jacquin, "Stability analysis and large eddy simulation of rotating turbulence with organized eddies," *J. Fluid Mech.* **278**, 175–200 (1994).
- <sup>20</sup>M. M. Rogers, "The structure of a passive scalar field with a uniform mean scalar gradient in rapidly sheared homogeneous turbulent flow," *Phys. Fluids A* **3**, 144–154 (1991).
- <sup>21</sup>T. Leweke and C. H. K. Williamson, "The long and short wave vortex pair instability," *Gallery Fluid Motion, Phys. Fluids* **8**, S5 (1996).